Atmospheric Environment 224 (2020) 117184

Contents lists available at ScienceDirect

Atmospheric Environment

journal homepage: http://www.elsevier.com/locate/atmosenv

Air pollution inputs to the Mojave Desert by fusing surface mobile and airborne *in situ* and airborne and satellite remote sensing: A case study of interbasin transport with numerical model validation

Ira Leifer [a,*], Christopher Melton [a], Robert Chatfield [b], Xinguang Cui [c], Marc L. Fischer [d], Matthew Fladeland [b], Warren Gore [b], Dennis L. Hlavka [e], Laura T. Iraci [b], Josette Marrero [b], Ju-Mee Ryoo [b], Tomoaki Tanaka [b], Emma Yates [b], John E. Yorks [e]

[a] *Bubbleology Research International, Solvang, CA, 93463, USA*
[b] *NASA Ames Research Center, Moffett Field, CA, 94035, USA*
[c] *Huazhong University of Science and Technology, Luoyu Road, 1037, Wuhan, China*
[d] *Lawrence Berkeley National Laboratory, 1 Cyclotron Road, Berkeley, CA, 94720, USA*
[e] *NASA Goddard Space Flight Center, Greenbelt, MD, 20771, USA*

HIGHLIGHTS

- Kern oil field's air flows through the Tehachapi Pass to the Mojave Desert.
- Mojave air quality can be reduced by fire to the north, through the Owens Valley.
- San Joaquin Valley and Los Angeles and fire pollution mix in the Mojave Desert.
- Climate change will increase the importance of fire air pollution to the Mojave.

GRAPHICAL ABSTRACT

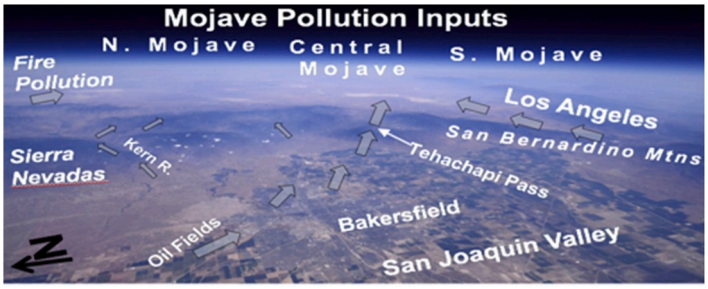

ARTICLE INFO

Keywords:
Methane
Flux estimation
Airborne campaign
Air basin
Fire
Smoke
Transport
Weather regional forecast model
LiDAR
Aerosol optical depth
COMEX

ABSTRACT

Deserts are fragile and highly sensitive ecosystems that increasingly are affected by upwind urban areas and industrial activities. The Los Angeles Basin (LAB) contributes to poor air quality in downwind deserts including the Mojave Desert. Few studies have investigated potential air pollution inputs to the Mojave, whose fragile ecosystem includes endangered plant and animal species.

Data were collected on 19 August 2015 by a mobile air quality laboratory, AMOG (AutoMObile trace Gas) Surveyor, that observed inputs can arise from the LAB as well as the San Joaquin Valley (SJV), California. The campaign used a strong methane (CH_4) plume as a tracer for the downwind fate of emissions from Bakersfield area petroleum production and also measured ozone (O_3). Additional *in situ* concurrent airborne GHG and O_3 data were collected by AJAX - Alpha Jet Atmospheric eXperiment. Both AMOG and AJAX measure winds.

Mojave Desert air quality was very poor (visibility ~4 km). Based on the winds, an additional source was inferred beyond the LAB and SJV Basins. Numerical transport modeling and analysis of aerosol lidar data collected the same day by the Cloud Profiling LiDAR onboard the Earth Research-2 stratospheric airplane

* Corresponding author.
E-mail address: ira.leifer@bubbleology.com (I. Leifer).

https://doi.org/10.1016/j.atmosenv.2019.117184
Received 2 October 2019; Received in revised form 17 November 2019; Accepted 23 November 2019
Available online 4 December 2019
1352-2310/

demonstrated that fires in Northern California were responsible, with prevailing winds transporting air southwards along the eastern Sierra Nevada Range (Bishop Valley) to the Mojave.

Whereas the southern and eastern Mojave are impacted by SJV and LAB outflow, the north Mojave generally avoids these inputs. This study shows it can be affected by even distant wildfires, which likely will increase in occurrence and intensity from climate change. Thus, regulatory efforts to reduce air quality impacts on the endangered Mojave ecosystem must include wildfires and also account for the significant differences between different regions of the Mojave. Currently, there is a paucity of studies, highlighting the critical need for field research.

1. Introduction

1.1. The Mojave Desert

The Mojave Desert is a vast (130,000 km^2), fragile arid ecosystem affected by a range of human activities including livestock grazing, linear structures such as roads that affect runoff, and air pollution (Lovich and Bainbridge, 1999). Recovery is slow – hundreds of years in the case of old Native American trade routes (Lovich and Bainbridge, 1999). Air pollution affects species composition, inducing a shift towards exotics over native perennials and annuals (Lovich and Bainbridge, 1999) and invasive grasses (Allen et al., 2014), primarily from deposition of ammonium nitrate aerosols and particles. Additionally, ozone (O_3) and other oxidant pollutants cause leaf injury, damaging grasses and large plants such as the Desert holly (Lovich and Bainbridge, 1999). Any changes in desert flora affects the fauna that depend on them for food and shelter. Given the desert ecosystem's harshness and sensitivity to precipitation and temperature changes, understanding air pollution stressors to the Mojave Desert (and other deserts) is important, particularly under warmer climate scenarios.

The second highest O_3 in California, after the Los Angeles Basin (LAB), is in the Mojave Desert. In large part this is because much of the Mojave Desert, most importantly the southern Mojave, lies downwind of both the LAB and the San Joaquin Valley (SJV) (Fig. 1). Beyond the Mojave, the LAB is a dominant southwestern US air pollution source. The LAB contributes to poor air quality as far downwind as the Colorado Plateau and Colorado River, 500–1000 km to the east (Bastable et al., 1990; VanCuren, 2015). The LAB also affects the Sonoran Desert to the

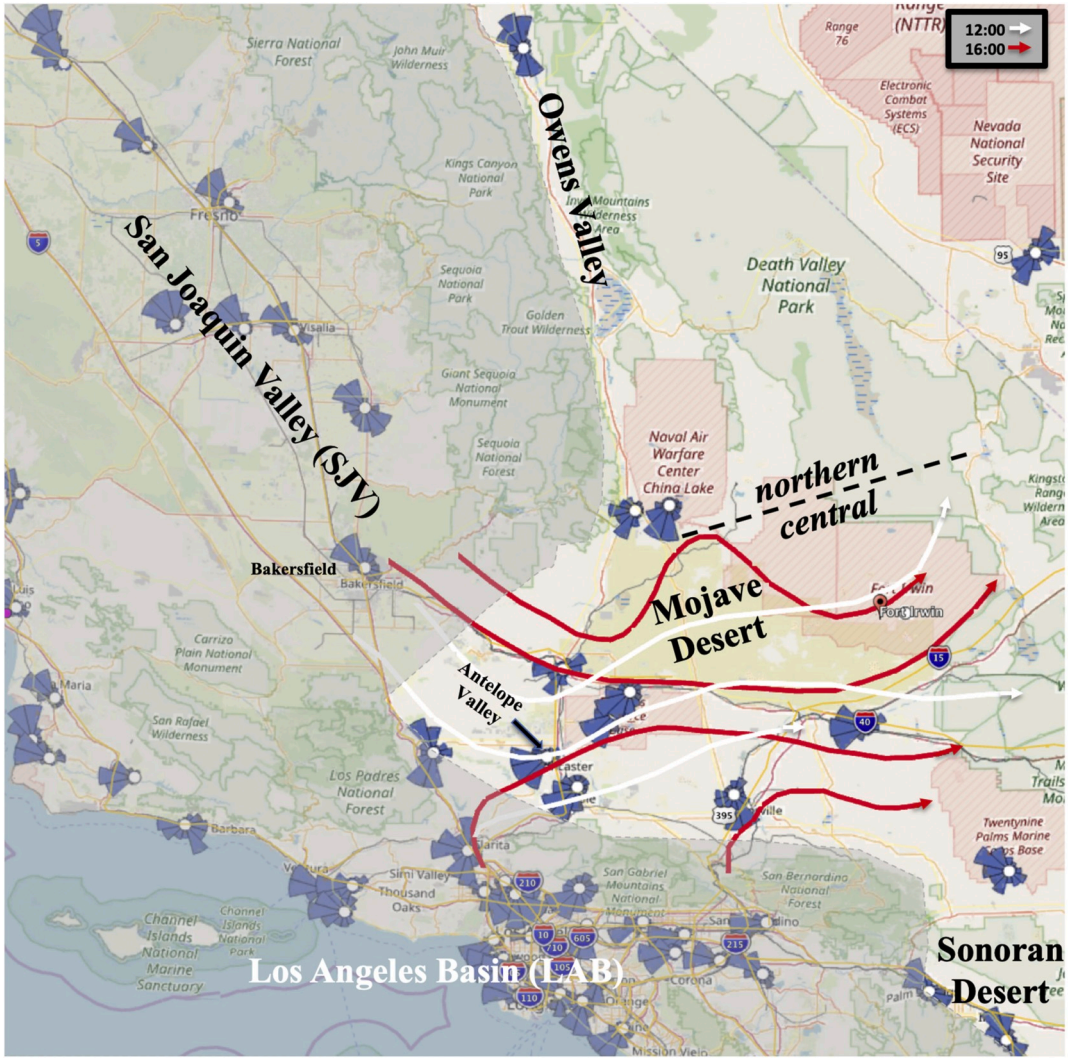

Fig. 1. Southwest California wind rose wind probabilities (full year) and typical Mojave Desert airflow for 1200 LT (Local Time) and 1600 LT, legend on panel, adapted from Trijonis et al. (1988). Non-desert areas darkened. Wind roses from www.windhistory.com.

south of the Mojave Desert. Parrish et al. (2017) looked at representative temporal trends in O_3 in the Mojave Desert and found that whereas the more remote portions remain pristine, areas affected by SJV and LAB outflows are highly polluted.

Central Mojave air pollution primarily originates from the SJV, which hosts most of California oil production, intensive agriculture, including concentrated dairies (Gentner et al., 2014) and major transportation arteries. To date, the transport of SJV pollution to the Mojave Desert remains very poorly quantified. Reible et al. (1982) conducted a tracer release experiment at Oildale (northwest of Bakersfield) and detected the tracer at China Lake (125-km downwind) in the Mojave Desert where air quality visibility is observed to worsen in the late evening and night. Trijonis et al. (1988) found a shift from LAB to SJV air pollution around Antelope Valley (Fig. 1) where the outflows converge.

Along with other California air basins, Mojave O_3 levels generally increased through ~1980, decreasing exponentially since with a 22 year e-folding time (Parrish et al., 2017). Much of the transport occurs in a layer ~1 km above mean sea level (the approximate altitude of the main mountain passes). This affects surface O_3 when afternoon mixing transports it to the surface.

1.2. Study motivation

In situ data collected by ground mobile and airborne platforms on 19 Aug. 2015 were combined to track a plume from Bakersfield area oil production in the SJV to the central Mojave where air quality was very poor – worse than in the Bakersfield area. To identify the source, airborne remote sensing aerosol observations acquired on 19 Aug. 2015 and satellite aerosol data were analyzed and identified wildfire smoke in northern California as the source. Numerical transport modeling confirmed the hypothesized southward air transport along the Bishop Valley, east of the Sierra Nevada Range.

A review of the rather limited literature on Mojave Desert air quality documented that Mojave Desert air pollution sources from the SJV and LAB, but did not find reports that distant wildfires can impact the Mojave Desert, as in this study. As such, wildfires represent an unassessed, sporadic, pollution source to the Mojave Desert, particularly the northern Mojave Desert. Given that wildfire frequency and intensity are anticipated to increase from climate change, this source and its impacts likely will increase. As such, these data support the need for a comprehensive, larger study that improves on efforts reported herein, both to establish a baseline and to assess air pollution budgets.

1.3. California air flow

California air basins tend to be stable with mixing depths significantly lower than the height of the mountain ranges that separate and isolate the air basins (Bao et al., 2008). Thus, prevailing westerly winds channel along valleys – mostly north-south oriented – and through mountain range passes (Trijonis et al., 1988). Air flows into the SJV from San Francisco Bay and then mostly moves southwards (Niccum et al., 1995). Southward flowing SJV air primarily escapes into the Mojave Desert through the Tehachapi Pass. (Leifer et al. (2018a)) found that transport also occurs through a pass near Breckenridge Mountain, located near the southern extension of the Sierra Nevada Range. Elsewhere, the Sierra Nevada Range blocks eastwards transport from the SJV including into the Mojave Desert.

Pacific air also reaches the Mojave Desert from the Oxnard Plains by way of the LAB. LAB air also escapes through passes into the Imperial Valley (Salton Trough) and the Mojave Desert (Leifer et al., 2016b). Bastable et al. (1990) found transport from the eastern LAB into the Mojave Desert in diurnal pulses lasting around 14-h flowing through the Cajon Pass.

1.4. Mojave Desert air flow

At high altitudes, winds generally flow across the Mojave Desert from the west-southwest; however, at lower altitudes, topography plays a critical controlling role (Fig. 1). One area where winds are complicated is along the eastern edge of the Sierra Nevada Range. Here, the often southward flowing air from Owens Valley pushes into the northwestern Mojave Desert in the afternoon (with air from south of China Lake pushing north, i.e., a counterclockwise circulation). There is seasonality in Owens Valley winds with winter winds generally to the north and summer winds generally to the south (Trijonis et al., 1988).

Air pollution at Edwards Air Force Base arrives approximately equally from the SJV and the LAB, with flow from the latter correlated with the worst visibility days (Trijonis et al., 1988). Prevailing winds generally transport this polluted air towards the south and southeast, impacting the south and east Mojave Desert.

Transport follows strong diurnal cycles, which manifest as diurnal cycles in visibility (Trijonis et al., 1988). Visibility is at a maximum in late morning as winds pick up and the mixed layer deepens. In the afternoon, further increasing winds decrease visibility as transport brings polluted air from the LAB and SJV. Further strengthening of winds in the late evening to late night improves visibility due to ventilation. There are seasonal cycles, with poor visibility in the fall and the worst visibility in the winter. In contrast, the northern Mojave Desert largely escapes the pollution from the LAB and SJV due to prevailing wind patterns. Thus, extreme gradients in air pollution are found across the Mojave Desert (Trijonis et al., 1988).

2. Approach

2.1. Experimental overview

Data were collected as part of the COMEX Experiment (CO2 and MEthane eXperiment) (Krautwurst et al., 2016). The *GOSAT-COMEX Experiment* (GCE) characterized greenhouse gas (GHG) emission on decameter (*in situ* surface) to kilometer (*in situ* airborne) to decakilometer (satellite) scales. GCE was developed to validate GHG emissions and columns directly derived from GOSAT (Greenhouse gases Orbiting SATellite) through fusion with *in situ* data that passes through all satellite pixels. *GCE* expanded on COMEX, evolving over the campaign. COMEX validated point-source plume inverse model derivation of GHG emissions from both *in situ* and remote sensing data (Krautwurst et al., 2016).

GCE protocol included an upwind surface *in situ* profile from the SJV floor (100-m AMSL - Above Mean Sea Level) to the crest of the Sierra Nevada Range (2-km AMSL) and a downwind profile to the Sierra Nevada Range crest. For this survey, data also were collected in the Mojave Desert to track the plume.

The AMOG Surveyor, described in Section 2.3.1, collected surface *in situ* data and was coordinated with AJAX (launched from the San Francisco Bay area), described in Section 2.3.2, were concurrent immediately downwind of the Kern Fields (Kern River, Kern Front, and Poso Creek oil fields). Airborne remote sensing of aerosol column data were collected by the Cloud Physics Lidar on the ER2 airplane, described in Section 2.3.3. Supporting satellite aerosol data were acquired from MODIS and supported by numerical air transport modeling, described in Section 2.3.4.

2.2. Study area

Data collection began with the Kern Fields, located adjacent to northwest Bakersfield (Fig. 2B). Bakersfield has the worst air quality in the United States for particulates (American Lung Association, 2019). Underlying this is that SJV winds generally are weak and there is little transport between adjacent basins (Bao et al., 2008) due to the Sierra Nevada range on the east, San Bernardino Mountains to the south, and

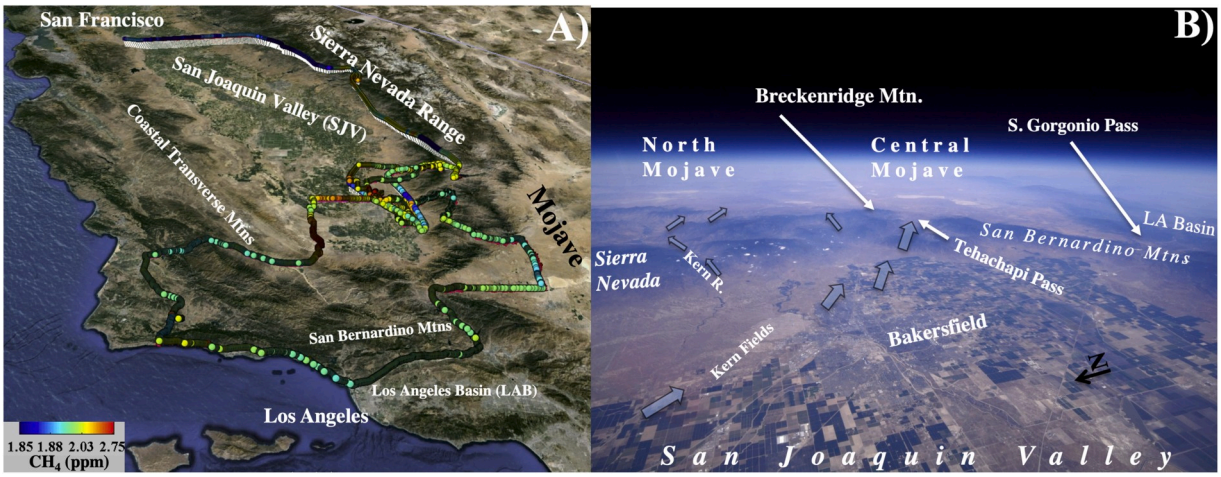

Fig. 2. **(A)** Full surface and airborne data for 19 Aug. 2015. Data key on panel. **(B)** Photo of Bakersfield and the South San Joaquin Valley from the ER-2 airplane at 20-km altitude. Approximate prevailing winds across the Kern oil fields and downwind and main features labeled. Photo courtesy Stuart Broce, Pilot, NASA Armstrong Flight Research Center.

Transverse Mountain Range to the west. What transport there is from the SJV to the Mojave Desert flows through passes in the south Sierra Nevada Range (Fig. 2B). The most important transport flow is through the Tehachapi Pass, but transport through passes near Breckenridge Mountain (Leifer et al., 2018a) and passes following the Kern River (Leifer, unpublished data, 2015) also have been documented. LAB airflow to the central and South Mojave passes through the San Gorgonio Pass (Leifer et al., 2016b).

Pollution sources in the south SJV include agriculture, husbandry, vehicular traffic (CA-99 corridor), Bakersfield urban emission, and fossil fuel industrial (FFI) production from the Kern Fields. On 19 Aug. 2015, air upwind of these oil fields was clean – low CH_4 – indicating air from the Sierra Nevada foothills, rather than the SJV floor where husbandry and agricultural emissions are mixed. In addition to CO_2 and CH_4, petroleum hydrocarbon production emits non-methane hydrocarbons (NMHC) (Katzenstein et al., 2003) and other trace gases.

The Kern Fields are a strong CH_4 source that largely is isolated from confounding plumes from other SJV CH_4 sources under prevailing winds, which transport plumes from other sources southwards, passing the Kern Fields to the west (Leifer et al., 2018a). The CA-99 traffic corridor was too far west for the observed wind flow to contribute to air quality at the Kern Fields. Furthermore, topographic steering ensures generally predictable, prevailing northwesterly winds across the Kern Fields. South of Bakersfield, winds shift to more westerly due to forcing by the San Bernardino Mountains. As SJV air reaches the eastern edge of the SJV, it flows through passes into the Mojave Desert (Fig. 2B). Overall, winds blow cross-slope (parallel to the mountain alignment) of the Sierra Nevada Range.

This study area includes complex wind flow patterns across and around the "toe" of Sierra Nevada foothills, which extend into the Kern Fields. Additionally, there is strong orographic forcing from tall bluffs (~100 m) on the Kern River Valley's south bank (Leifer et al., 2018a), which also separate the Kern Fields from the city of Bakersfield (pop. 364,000 in 2013).

FFI emissions affect and interact with oxidant pollutants, such as O_3, which affects human health (Jerrett et al., 2009) on urban and regional scales. Specifically, O_3 production is sensitive to NO_X and volatile organic hydrocarbons (VOH) concentrations (such as emitted by FFI activity) (Mazzuca et al., 2016). Ahmadov et al. (2015) found interaction with reactive odd nitrogen (NO_y, defined, $NO_y = NO+NO_2 + NO_z$) and sulfur dioxide with VOH from FFI production, leading to increased O_3.

Although upwind air was not recently from agricultural sources, the plume passed over agricultural land southeast of Bakersfield. SJV agriculture is intensive, with significant ammonia gas emissions from fertilizer applications and CH_4 from irrigation ditches, holding ponds and agricultural infrastructure; however, dairies are absent along the plume's pathway.

Traffic adds NO_X to VOH from FFI and NH_3 from agriculture. Note, the Tehachapi Pass to the Mojave also is a major traffic corridor. This, in combination with solar insolation (typical for the Mojave Desert), leads to photochemical aerosol generation (Pandis et al., 1992).

2.3. Platforms

2.3.1. AMOG surveyor

In situ surface data were collected by the AMOG (AutoMObile greenhouse Gas) Surveyor mobile analytical laboratory (Fig. 3A), which was developed for mobile high-speed observations of trace gases, winds, temperature, aerosols, and solar spectra. AMOG Surveyor includes a range of fast-response Cavity Enhanced Absorption Spectroscopy (CEAS) analyzers (Leen et al., 2013) and slower fluorescence analyzers that measure 13 trace gases – mostly at sub-ppb levels.

AMOG Surveyor uses a high flow vacuum pump (850 L min^{-1}) to draw samples down Teflon® sample lines from 5 to 3 m above ground into a cavity enhanced absorption spectrometer (CEAS) (FGGA, Los Gatos Research, CA), which measures CH_4 and CO_2, and a fluorescence analyzer (42c, ThermoFischer Scientific, MA) that measures O_3. CH_4 and CO_2 are calibrated before surveys with a greenhouse gas air calibration standard (CH_4: 1.981 ppmv; CO_2: 404 ppmv). The O_3 analyzer was calibrated at NASA Ames with the same O_3 calibrator (2B Tech Model 306) used for the AJAX O_3 analyzer. Recent AMOG Surveyor improvements now allow measurement of 14 trace gases, 3D winds, aerosol size distributions, and vertical aerosol profiles.

AMOG Surveyor operates at up to highway speed, implementing an adaptive surveying strategy (Thompson et al., 2015) by real-time analysis and visualization. In particular, fast analyzer data and winds allows adjustment of the survey route and speed, thereby increasing data density in areas of interest (Leifer et al., 2016b). For further AMOG details, see Leifer et al. (2018a); Leifer et al. (2016a); Leifer et al. (2014); Leifer et al. (2018b); and Leifer et al. (2019).

2.3.2. AJAX

AJAX (Fig. 3B) collected airborne *in situ* measurements of CO_2, CH_4, H_2O by cavity ringdown spectroscopy (G2301-m, Picarro Inc.) and O_3 (Model 205, 2B Technologies Inc.), and meteorological parameters including 3D winds (Meteorological Measurement System, MMS). AJAX flies at an average speed of 490 km h^{-1}, providing a snapshot of

Fig. 3. Study platforms. **A)** AutoMObile trace Gas (AMOG) Surveyor on the Kern Bluffs south of the Kern River oil field. Photo Ira Leifer. **B)** The AlphaJet Atmospheric Experiment (AJAX) fighter jet, photo courtesy Akihiko Kuze, Japanese Space Agency, JAXA. **C)** Photo of the Cloud Physics LiDAR (CPL).

atmospheric winds and plume structure. The greenhouse gas analyzer is calibrated using NOAA whole-air standards; calibrations are performed before and/or after each flight with the calibration factor closest to the day of flight being applied to each raw CO_2 and CH_4 measurement. Further corrections include applying water vapor corrections provided by Chen et al. (2010) to calculate CO_2 and CH_4 dry mixing ratios. Data also are filtered for quality control for deviations in instrument cavity pressure or temperature. On this flight, no deviations in pressure were observed; data during the return leg were discarded due to overheating ($T > 45.15$ °C).

2.3.3. Cloud Physics LiDAR

The Cloud Physics LiDAR (CPL) (Fig. 3C) is a multi-wavelength backscatter LiDAR operating at 1064, 532, and 355 nm for airborne deployment (McGill et al., 2002). The CPL provides high temporal-resolution (200-m along track) at high vertical-resolution (30-m for cloud profiling). On 19 Aug. 2015, the CPL was flown on the NASA Earth Research-2, high-altitude airplane. The CPL collected data over Central and Northern California and Western Nevada (and the Pacific) and included data collected over the Sierra Nevada Range (3-h concurrence with AMOG at Alta Sierra), across the SJV and across the active massive fires near the Oregon-California border.

2.3.4. Numerical air transport model

The Weather Research and Forecasting (WRF) model version 3.6.1, with time averaging adapted for atmospheric trace gas transport over California (Nehrkorn et al., 2010; Skamarock et al., 2008) was used to predict the source of air in the Tehachapi Pass outflow in the Mojave Desert based on back trajectory calculation. Boundary and initial conditions were extracted from the North American Regional Reanalysis dataset (NARR) (Mesinger et al., 2006). Here, WRF used 50 vertical levels to minimize errors in boundary layer meteorology over California's complex terrain. 27 layers are within the atmosphere's lowest 3 km (Jeong et al., 2013). The land surface was parameterized using a five-layer thermal diffusion model (see Ruiz et al. (2010) for details) to capture the effects of agricultural irrigation during summer months, and the unified NOAH-MP LSM (Multiparameter Land Surface Model (Chen and Dudhia, 2001). We used the Yonsei University (Hong et al., 2006) parameterization for boundary layer physics, which includes an improved representation of topographic influences on boundary layer flows (Jiménez and Dudhia, 2011). We consider this relevant for the southern end of the Central Valley. Each day is computed separately over a 30-h run with an initial 6-h spin-up (Pillai et al., 2011).

Air parcels were tracked back in time using the WRF-STILT (Stochastic Time-Inverted Lagrangian Transport) model (Jeong et al. (2013) and Cui et al. (2019)). A total of 500 particles were released from three receptor locations in the Tehachapi Pass outflow in the Mojave Desert that span the alluvial fan of the pass, and back propagated 72 h. These sites were at 850–900 m altitude. Particle spread is from stochastic mixing along the trajectories.

3. Results

3.1. Upwind air

AMOG Surveyor collected upwind profile data during an ascent and descent ~50-km north of the Kern Fields. AMOG's descent was ~1 h prior to the descent profile collected by AJAX (Fig. 4). SJV floor surface and airborne winds were northwest (aligned with topography), featuring an upslope flow towards the pass by both AJAX and AMOG. The PBL was determined to be at 1600 m from AJAX and AMOG temperature (T) profiles and AMOG CH_4 profiles. From Alta Sierra, the AMOG driver noted poor air visibility – rather unusual for the high Sierra Nevada – compared to lower in the SJV. Both *in situ* platforms noted elevated O_3 above the PBL - AMOG observed nearly 100 ppb during a pause in an open grassy field (i.e., not forested) on the ridge crest. Further profile details and a comparison between AMOG and AJAX winds that showed good agreement after filtering AMOG wind data are described in Leifer et al. (2018b).

3.2. Kern Fields' CH_4 plume trajectory

On 19 Aug. 2015, Kern Fields' winds were prevailing (northwesterly) and fairly strong (~3 m s^{-1}) at the surface and somewhat stronger aloft (Fig. 5). Observations showed that surface topography, e.g., the Kern River bluffs, modifies winds both at the surface and at altitudes of 1-2 km (Leifer et al., 2018b). Southeast of Bakersfield, winds veered to westerly's and towards passes to the Mojave Desert in the Sierra Nevada. Winds across the Kern Fields were ~3.5 m s^{-1} (12 km h^{-1}) from 1230 to 1400 LT (Fig. 5). Earlier winds (~0930 LT) around Delano were weaker and from the north (Fig. 4A). Under these wind conditions, agriculturally-sourced CH_4 passed to the west of the Kern Fields during the study. Winds far downwind (~50 km) of the study area (1530 LT, several hours later, approximately Lagrangian) near the small towns of Edison and Arvin (Fig. 6A) showed the Kern Field's CH_4 plume drifting towards the Tehachapi Pass. Here, AMOG plume transits are on agricultural roads with negligible to no traffic.

AMOG's southward transit descended from Breckenridge Mountain to Caliente, CA, and then ascended to the Tehachapi Pass, where the highest CH_4 concentrations of this southwards transit were observed.

Notably, enhanced CH_4 was absent in the pass to the north of Breckenridge Mountain (Fig. 6A). Although visibility in the Tehachapi Pass was good, the descent from the Tehachapi Pass to the Mojave Desert, featured rapidly worsening visibility, estimated at ~4 km in the Mojave Desert. During the winding descent from Tehachapi, winds often aligned with traffic, confounding surface measurements, e.g., highly localized, strong CO_2 anomalies (Fig. 6C, **white arrows**). Descent CH_4 showed a smooth downwind decrease consistent with SJV air mixing through the Tehachapi Pass into the Mojave Desert. This wind flow is nearly straight line from Bakersfield across the south SJV (Fig. 6A, **pale white dashed line**). A north-south transect captured the SJV outflow plume (Fig. 6B). This was under very strong crosswinds on the highway's upwind side, which prevented vehicular data contamination –

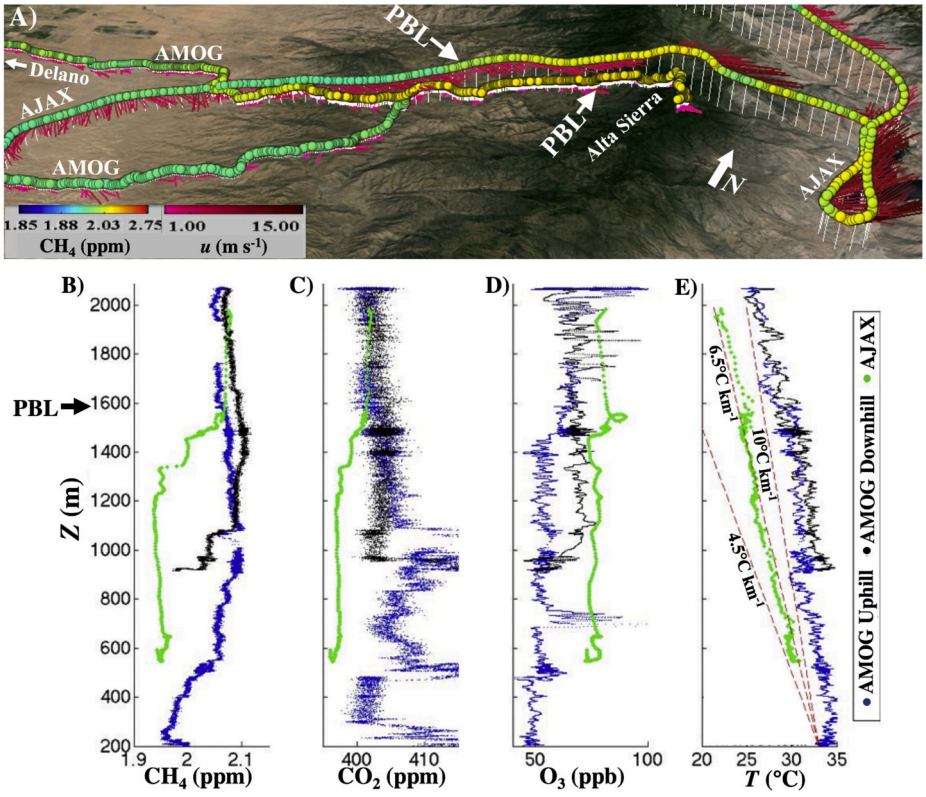

Fig. 4. Upwind data for **A)** AJAX and AMOG *in situ* methane (CH_4) and winds (u). Circle color shows CH_4 concentration, red lines show wind direction, color indicates wind speed. Airborne CH_4 and wind data are at measurement altitude. Surface CH_4 data height is proportional to CH_4 concentration. Profiles for **B)** CH_4, **C)** carbon dioxide (CO_2), **D)** ozone (O_3), and **E)** temperature (T) and adiabatic lapse rates. Data key on figure. (For interpretation of the references to color in this figure legend, the reader is referred to the Web version of this article.)

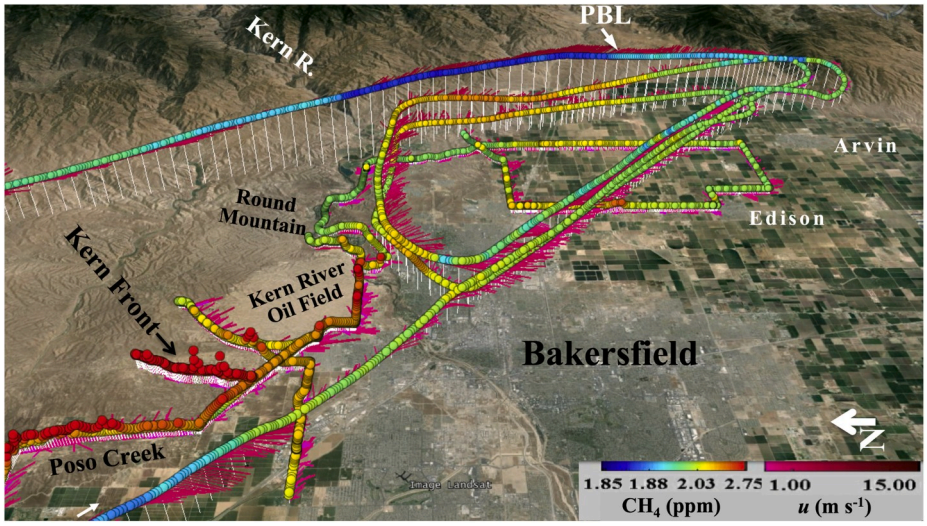

Fig. 5. AJAX and AMOG *in situ* methane (CH_4) and winds (u) for 19 Aug. 2015. Circle color shows CH_4 concentration, red lines show wind direction, shade of red indicates wind speed. Airborne CH_4 and wind data are at their measurement altitude. Surface CH_4 data height is proportional to CH_4 concentration. Data key on figure. (For interpretation of the references to color in this figure legend, the reader is referred to the Web version of this article.)

primarily CO_2 (Fig. 6C).

A second, distinct, eastward-flowing plume of CH_4 and CO_2 enriched air was encountered further south in the Mojave Desert (Fig. 6C). AMOG saw similar, high CO_2 air exiting the I-5 pass where southerly winds were advecting air from the San Fernando Valley (part of the LAB) into the Mojave Desert. Upon exiting the I-5 pass, westerly winds drive the plume eastwards; however, *in situ* data are unreliable under strong tailwinds. These two plumes flow into clean Mojave air, mixing with and displacing the clean air.

Based on the north-south CH_4 gradient, the LAB and SJV outflows first touch slightly north of Rosamond, where CH_4 reaches a minimum. This pattern agrees with Reible et al. (1982) regarding the outflow behavior of these two air basins.

To understand the source air masses of the air observed in the central western Mojave Desert, the ratios of CH_4:CO_2 were investigated for data collected by AJAX and AMOG. The analysis segregated data spatially and identified some clear characteristics, with quite different fingerprints for the northern air mass and southern air mass in the Mojave Desert (Fig. 7A and B) in AMOG data. The difference arises from the shift between LAB and SJV sources, with the former enhanced in CO_2 relative to CH_4. SJV air includes significant input from oil and gas production, which tend to enhance CH_4 relative to CO_2. AJAX SJV data (Fig. 7C)

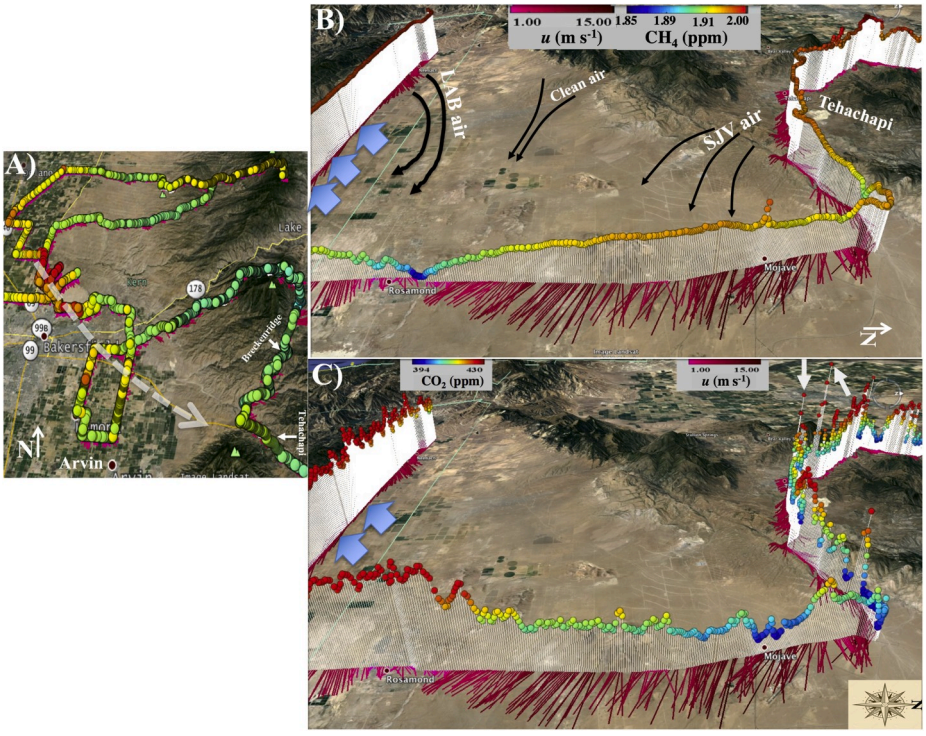

Fig. 6. A) AMOG *in situ* methane (CH_4) and winds (u) showing plume advection towards the Tehachapi Pass (white dashed arrow). Circle color shows CH_4 concentration, red lines show wind direction, shade of red indicates u.. **B)** CH_4 and winds. Black arrows show overall transport paths for LAB and SJV outflow plumes. Blue arrows identify potentially contaminated air. **C)** AMOG CO_2 surface data for the Tehachapi Pass outflow into the Mojave Desert. White arrows show examples of CO_2 vehicular emissions during the Tehachapi Pass descent. Data key on panels. (For interpretation of the references to color in this figure legend, the reader is referred to the Web version of this article.)

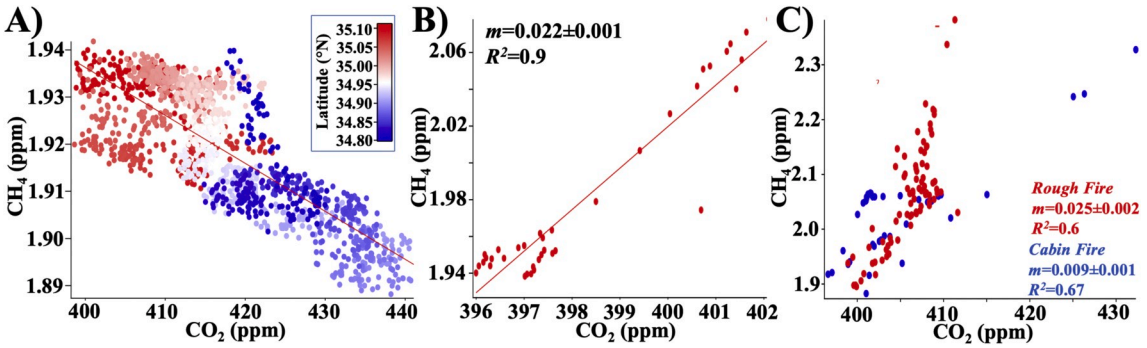

Fig. 7. AMOG surface methane (CH_4) versus carbon dioxide (CO_2) for Mojave Desert data with respect to **A)** latitude. Data key on figure. B) AJAX data collected near AMOG Surveyor data for the Kern Fields area CH_4 versus CO_2 and **C)** AJAX data for the Cabin and Rough Fires and CH_4 versus CO_2. Fit slopes, m, shown for panels A, B).

were typical of northern Mojave AMOG data, where SJV influence is expected, lying in the upper left of Fig. 7A. The negative trend in AMOG CH_4 versus CO_2 is from mixing and thus disagrees with the AJAX CH_4 versus CO_2 trends for SJV.

Fortuitously, AJAX also collected fire data, which showed enhanced CH_4 compared to CH_4 versus CO_2 for both the Cabin and Rough fires, notably steeper for the Rough fire. CH_4 for the fire data lie well above the AMOG data (Fig. 7A) suggesting the air responsible for the poor Mojave visibility was aloft where AMOG surveyed, i.e., AMOG should have surveyed further downwind to sample it.

3.3. Mojave Desert and fire aerosols

Important air pollution sources to the western Mojave Desert are from the LAB and the SJV (Bastable et al., 1990). These sources have significantly elevated pollution and greenhouse gas concentrations compared to the Mojave Desert - AMOG measured 1.88–1.89 ppm CH_4 in Death Valley (Leifer, unpublished data, 2015). However, these could not explain the poor air visibility, which strongly suggested an alternative source. Moreover, circa 100 km to the north at Sierra Alta on the crest of the Sierra Nevada Range and above the PBL, poor visibility was observed visually, with AJAX observing elevated CO_2, with both platforms observing elevated O_3 (Fig. 4).

These data and observations suggested a wildfire source and advection from the north. A number of large wildfires were active across the western US with major fires in the Pacific Northwest and northern and central California (Fig. 8). These fires included, the Cabin Fire, which was active in the central California Sierra Nevada (34.25N, 117.85W, started 14 Aug. 2015). Eventually, the Cabin Fire burned 1723 acres until contained completely on 20 Aug. 2015 (http://inciweb.nwcg.gov/incident/4413/).

MODerate Imaging Spectroradiometer (MODIS) satellite imagery (Fig. 8B) suggested eastwards advection of most of the Cabin Fire's smoke, with the plume fanning out both north and south into the northern Mojave Desert. Additionally, some of the Cabin Fire smoke also appears to be advected southwards, overlapping with AJAX's flight path. Where AJAX overlapped the smoke in MODIS, elevated CH_4 (to 2.2 ppm) was observed. In contrast, CH_4 concentrations south of the

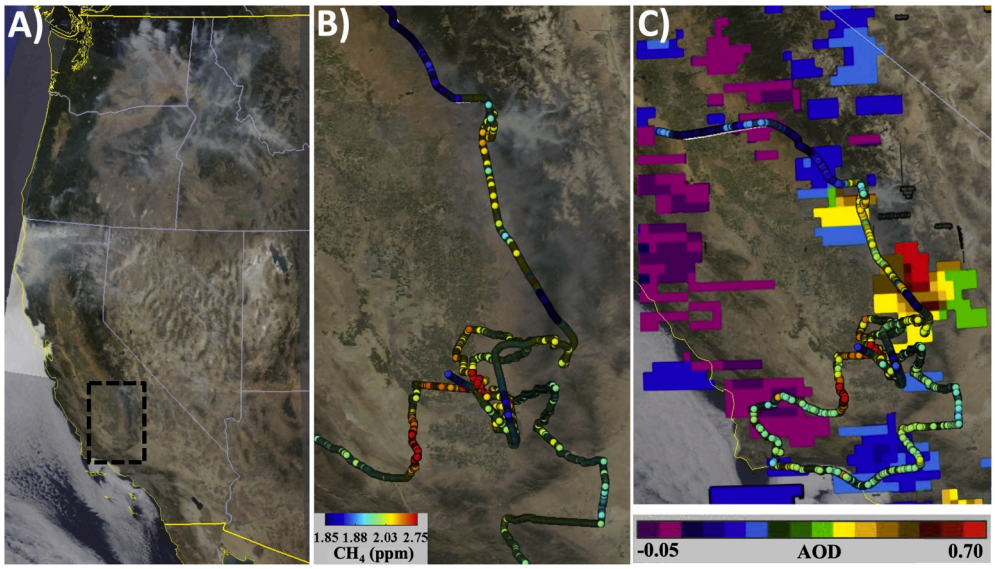

Fig. 8. **A)** MODIS Terra RGB imagery from 19 Aug. 2015, from http://ge.ssec.wisc.edu/modis-today/. Black square shows focus area. **B)** MODIS Terra imagery of the focus area and *in situ* CH_4 AMOG and AJAX data. **C)** MODIS Aerosol Optical Depth (AOD) and full methane (CH_4) dataset. MODIS AOD was from the MOD04 Collection 6 Algorithm, combined product (Levy et al., 2013), 1825 UTC overpass. Data key on figure.

Cabin Fire were not elevated, where smoke was absent. This co-location with the smoke strongly suggests southwards transport.

The potential for southerly transport was provided by inspection of winds retrieved from the HRRRv2 (High Resolution Rapid Refresh) archive (Alexander et al., 2011). The winds suggest smoke transport into the Sierra Nevada Range (Fig. 9). Based on MODIS Aerosol Optical Depth (AOD) maps, smoke aggregated to the north of Alta Sierra, with a pattern that suggests eastwards transport into the Mojave Desert (Fig. 8C). MODIS AOD retrievals were challenged by the terrain in the Mojave Desert, capturing some, but missing much of the visible smoke in the MODIS visible imagery (Fig. 8B). These MODIS data agree with AMOG visual observations from Alta Sierra of poor air quality over the Mojave Desert and from Tehachapi Pass and with the visual observations of the AJAX pilot.

MODIS suggested (Fig. 8A) a strong fire smoke plume flowing across the Sierra Nevada eastward at least as far as into the northern Nevada high desert. Further characterization of air quality in the Mojave Desert and towards the north into Nevada was provided by the Cloud Physics LiDAR (CPL), which flew on the NASA Earth Research-2, high-altitude airplane, and was nearly coincident (within 3 h) of AMOG at Alta Sierra. CPL data (Fig. 10) included a flight over the large fires near the northern California–Oregon border, where it observed high aerosol backscatter in a thick layer extending up to 5-km altitude, particularly in northern California. On the southwards leg, aerosol AOD gradually decreases towards the south on the southwards leg, with the layer largely maintaining its thickness (~5 km). CPL data are consistent with this plume being transported eastwards into the high desert of western Nevada, with aerosol backscatter gradually decreasing towards the south, suggesting aerosol input to the northern Mojave Desert (Fig. 10). These interpretations are consistent with the interpretation of the MODIS imagery.

Additional smoke aerosol input from the Cabin Fire is apparent near the southern-most extent of the north-south flight leg (Fig. 10, **green arrow**).

3.4. Numerical simulation to identify air source

Back trajectories were calculated with the WRF model for three receptor locations in the Mojave Desert at the Tehachapi Pass Outflow (35.14°N, 118.17°W, 35.11°N, 118.17°W, 35.06°N, 118.17°W). These receptor sites were chosen to span the alluvial fan. A total of 500 particles were released from these three receptor sites at each altitude and

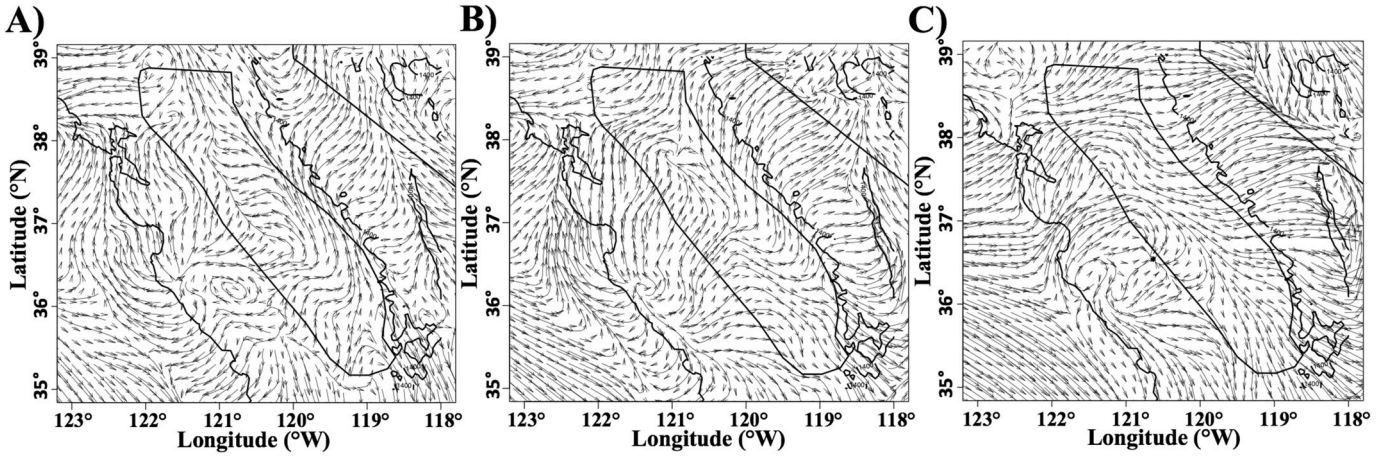

Fig. 9. High Resolution Rapid Refresh winds for 1390 m altitude for **A)** 0800, **B)** 1100, and **C)** 1400 local time, 19 Aug. 2015.

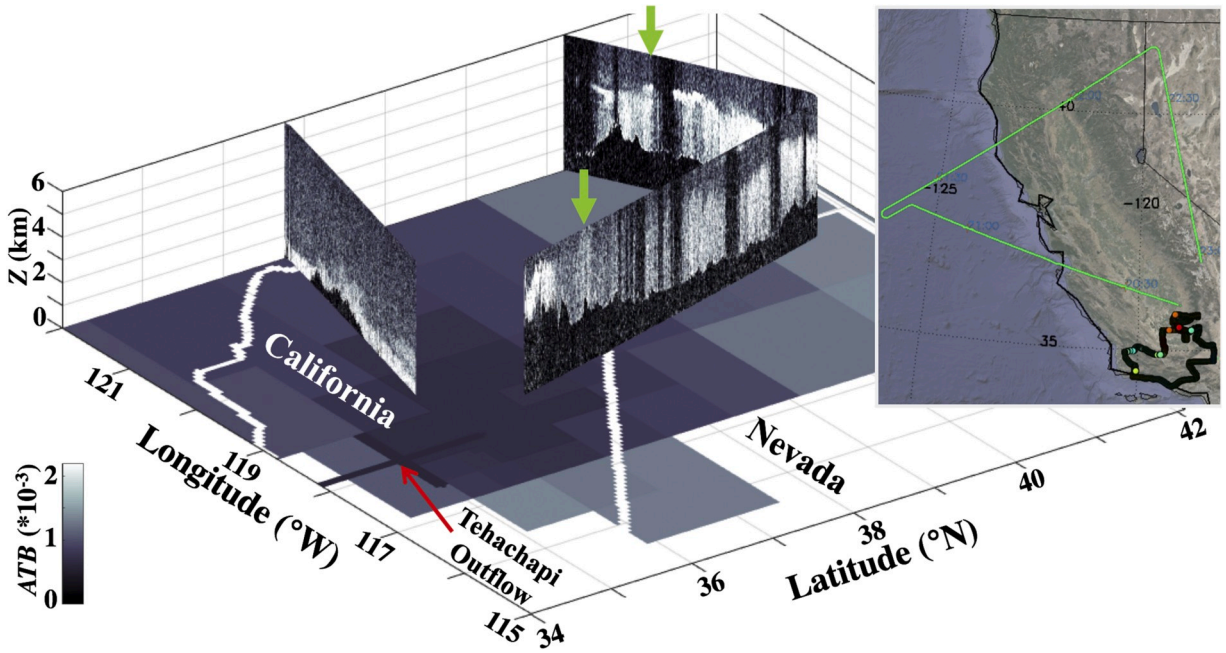

Fig. 10. Cloud Profiling LiDAR (CPL) attenuated total backscatter (ATB) for 532 nm, over Sierra Nevada and southern California for 19 Aug. 2015 and 72-h surface gridded back trajectories shown on surface (Fig. 12). CPL flight path (see inset) intersected with Cabin Fire smoke plume (green arrow). Inset shows flight path and AMOG data. ATB data key on figure. (For interpretation of the references to color in this figure legend, the reader is referred to the Web version of this article.)

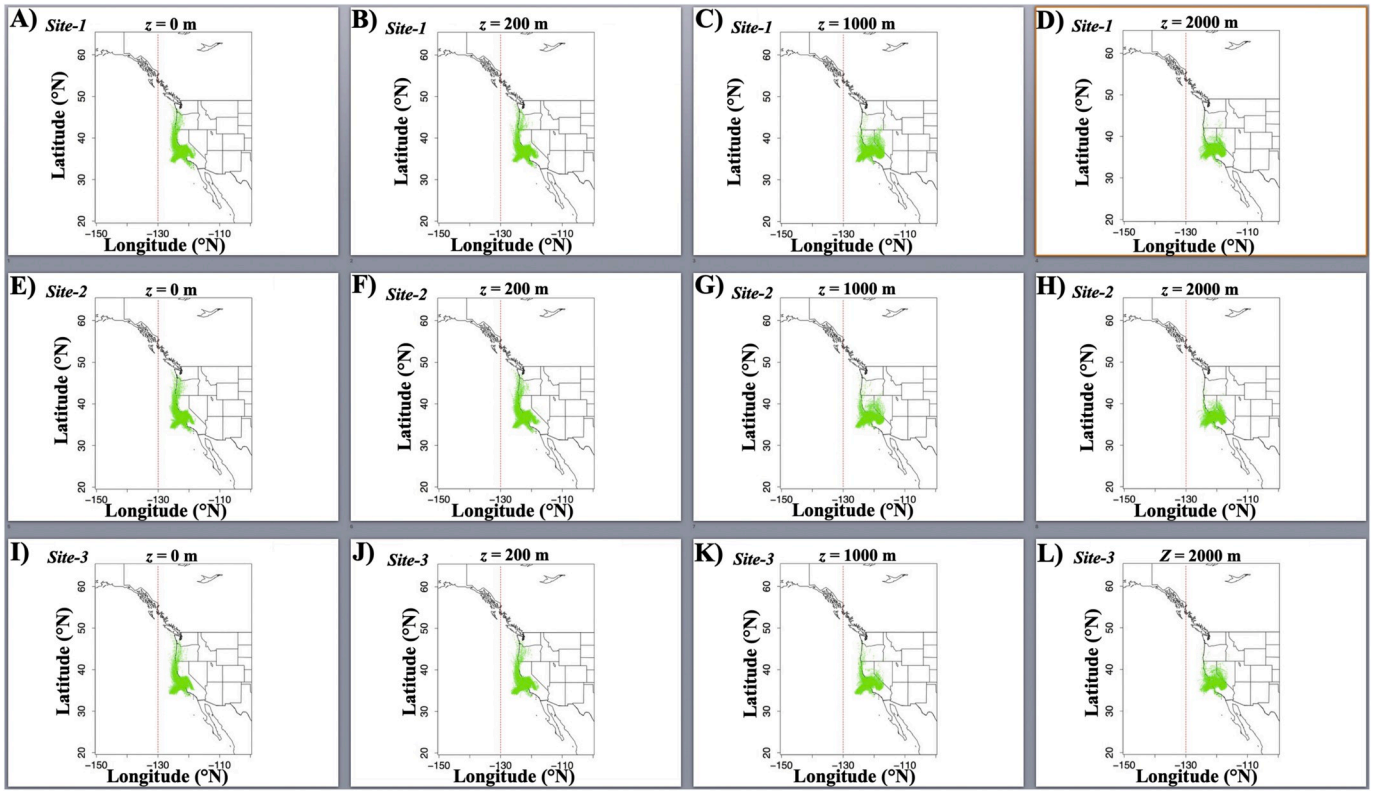

Fig. 11. Calculated, 72-h back-trajectory origins, for 19 Aug. 2015 for Site 1–35.14°N, 118.17°W, Site 2–35.11°N, 118.17°W, and Site 3–35.06°N, 118.18°W for heights (*z*) 0, 200, 1000, and 2000 m for 500 particles. Sites and heights labeled on panels.

the original location of each particle 72 h prior was determined and is shown in Fig. 11. A map of the number of particles arriving from each grid cell is shown in Fig. 12.

The simulations showed that near the surface, air from the Tehachapi Pass had largely arisen from the Pacific Ocean, transiting the San Francisco Bay into the SJV and then south, exiting the SJV at its southeast edge (Fig. 11A, 11E, 11F; 12A, 12E, 12F). Surface air for all three sites arrived from similar locations. In contrast, air at 1000 m included a contribution from both along a lengthy stretch of the Pacific Coast and also the Mojave Desert and other regions to the north

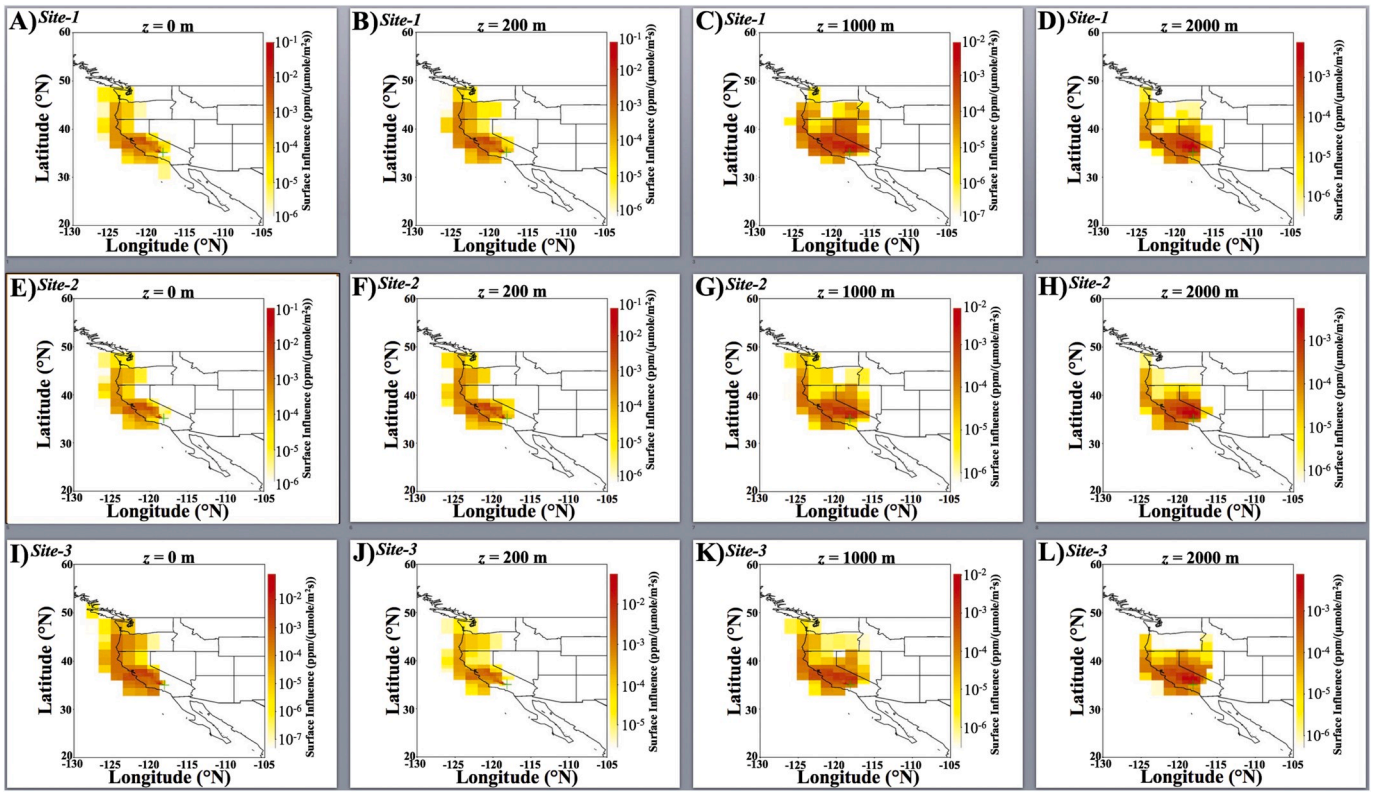

Fig. 12. Calculated, 72-h back-trajectory gridded contribution - number of particles arriving from each grid cell for 19 Aug. 2015 for Site 1–35.14°N, 118.17°W, Site 2–35.11°N, 118.17°W, and Site 3–35.06°N, 118.18°W for heights (*z*) 0, 200, 1000, and 2000 m. Sites and *z* labeled and data keys on panels.

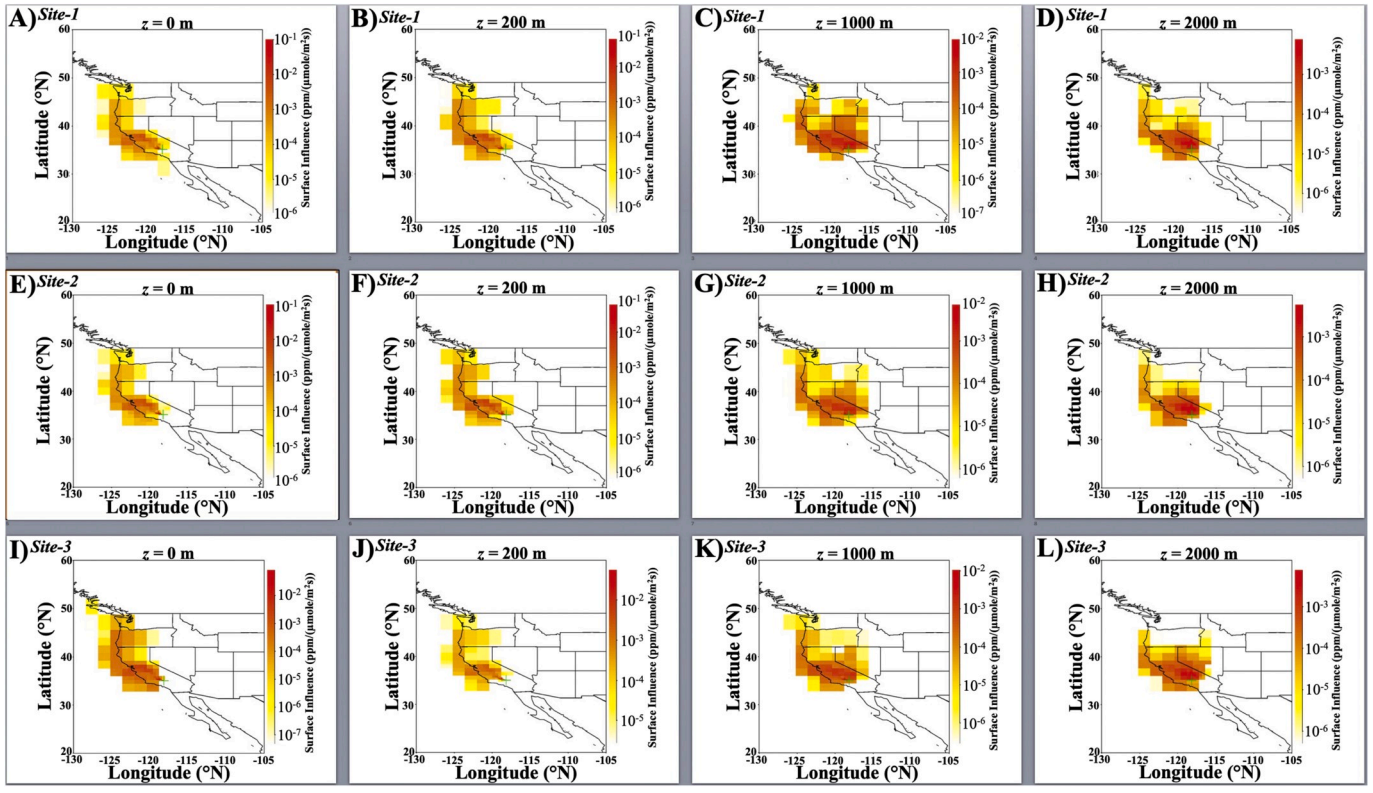

Fig. 13. Numerically simulated 72-h back trajectory for air parcels at 35.14°N, 118.18°W (Mojave Desert, Tehachapi outflow, circles) for **A)** surface and **B)** 2000 m altitude, and surface contribution. White arrow shows three receptor sites.

(Fig. 11C, 11G, 11K; 12C, 12G, 12K). There was a significant difference at 1000 m between the origin of air on the northern edge of the fan from on the southern edge of the fan, Specifically, Mojave Desert air for the northern receptor site came from far further north, near the Oregon border, than for the southern receptor site (Site 3), where the air sourced from only as far north as Reno (Fig. 11K; 12K). For 2000 m, there was far less input from along the California Coast (Fig. 11D, 11H, 11L; 12D, 12H, 12L); with the same trend as for 1000 m with respect to how far to the north the air had originated from. Air at 200 m came from similar locations to surface air, distinct from 1000 m, indicating that the mixed layer extends to somewhat less than 1000 m.

The particle origins then were gridded to derive the relative contribution from different areas to the air at the receptor sites (Fig. 13, **white arrow**). The WRF model simulations showed that surface air in the Tehachapi Pass outflow exclusively came through the pass from the SJV. Moreover, its origin was largely from the coastal Pacific Ocean, entering the SJV through the Bay Area (Fig. 13A). This is a typical inflow pattern for the SJV. In contrast, the simulations show a transition in the source location between 200 and 1000 m altitude. Given the receptor site altitudes were at 900 m, a transition at ~750 m above the surface would be expected for an isobaric flow through the pass based on the PBL thickness in the SJV. Air at 2000 m was sourced from both the SJV and the Mojave Desert, and from regions further to the north, with the strongest contribution arising from the area around the Cabin Fire. Thus, the simulations support the interpretation of the MODIS data, CPL data, *in situ* data, and visual observations – there was a significant non-coastal contribution from the north.

4. Discussion

4.1. Pollution sources to the Mojave Desert

Based on its lack of industry, population, agriculture, and wetlands, the Mojave Desert should feature extremely clean air, yet, stubbornly remains in violation of air quality standards (Parrish et al., 2017). This has significant impacts on the ecologically sensitive desert environment (Allen et al., 2014).

Mojave Desert air pollution largely arises from its two upwind air basins – the SJV and the LAB (Trijonis et al., 1988). Flow between these basins largely is constrained to mountain passes, which are poorly aligned with the prevailing westerly, high-level winds over southern California. Air from the San Fernando Valley in the western LAB also flows into the Mojave Desert through several north-south passes that traverse the San Bernardino Mountains. Upon outflowing into the Mojave Desert, the plume (defined by the passes) flows eastward under prevailing winds, which are aligned with the east-west San Bernardino Mountains. The orientation of the SJV is near orthogonal to the prevailing winds, except at its southern extent, which is defined by the San Bernardino Mountains. Reible et al. (1982) found inter-basin airshed transport through the Tehachapi Pass during a tracer release study at Oildale (near Bakersfield and the Kern Fields) with the tracer detected near the towns of Mojave and China Lake in the Mojave Desert.

Based on the north-south CH_4 gradient (Fig. 7), this suggests that the LAB and SJV air outflows into the clean Mojave air intersected slightly north of Rosamond on 19 Aug. 2015, where CH_4 reaches a minimum – Moreover, CO_2 and CH_4 clearly are significantly different between these air basins. These observations are consistent with observations that half the pollution at Edwards Air Force Base arrives from the SJV (Reible et al., 1982; Trijonis et al., 1988). Generally, prevailing winds transport this polluted air towards the south and southeast Mojave Desert.

Transport follows strong diurnal cycles, which manifests as diurnal cycles in visibility (Trijonis et al., 1988). Visibility is at a maximum in late morning as winds pick up and the mixed layer deepens. In the afternoon, further strengthening winds lead to decreased visibility as transport brings polluted air from the LAB and SJV. AMOG Surveyor arrived in the Mojave Desert late afternoon during the period of strong transport. Later, further wind strengthening in the late evening to late night improves visibility due to ventilation.

There also are seasonal cycles, with poorest visibility in mid-summer, asymmetrically extending into the fall. This summer visibility minimum corresponds to a peak in aerosol organics, whereas sulfate aerosols peaks in early fall, and soil aerosols peaks in late spring. The latter corresponds to windiest season (Trijonis et al., 1988).

In contrast, the north and northwest Mojave largely escapes from LAB and SJV pollution for typical wind flow patterns. This creates extreme air pollution gradients across the Mojave Desert (Trijonis et al., 1988). As such, characterization by a single temporal trend, e.g., Parrish et al. (2017), may inaccurately represent temporal air quality trends in different portions of the vast (130,000 km^2) Mojave Desert.

One source of worsening air quality in the north and northwest Mojave is wildfires (both local and distant) as demonstrated herein for long-range transport of wildfire pollution. Wildfire air pollution mixes with the SJV and LAB outflows, further complicating smog chemistry and potentially compensating for oxidants and VOH reductions due to regulations in the SJV and LAB. As such, partitioning the Mojave Desert into two or more air basins (tentatively between Fort Irwin and China Lake) would provide a better basis for evaluating air quality trends. It should be noted that wildfires are an intermittent, albeit often persistent and frequent, source. Moreover, the wind conditions in this study that brought northern California wildfire smoke to the northern Mojave Desert are frequent (Fig. 1), particularly during summer (Trijonis et al., 1988).

The atmospheric chemistry where the LAB and SJV air outflows mix is significant because whereas SJV is NH_3 rich (Clarisse et al., 2010), LAB, as with many megacities, is rich in oxidant trace gas species. This combination facilitates the formation of ammonium aerosols, which then dry deposit into soils (Pinder et al., 2008), affecting flora (see below).

4.2. Ecosystem implications

Ammonium nitrate deposition favors non-desert species and grasses (Allen et al., 2014), affecting the higher species of the food chain. As a result, desert fires are more common in areas of higher nitrogen deposition where invasive grasses grow profusely (Allen et al., 2014). Additionally, O_3 affects plant and animal health (Lovich and Bainbridge, 1999). In the fragile desert ecosystem, these impacts are significant. Although O_3 in California has been decreasing over recent years in some parts of the Mojave Desert (Parrish et al., 2017), in other parts, O_3 and NO_X have been stable, whereas statewide NH_3 is forecast to increase (Cox et al., 2013). Still, NH_3 in the SJV is in excess of NO_X for ammonium nitrate formation (SJVUAPCD, 2015). Thus, mixing with NO_X from the LAB outflow (NO_X emissions from LAB are double those of the SJV) in the Mojave Desert will lead to further NH_3 transformation into ammonium aerosols.

4.3. Implications of warmer climate scenarios

Export of LAB and SJV pollution depends on the strength and timing of winds and also PBL thickness – a thicker PBL allows more air to escape through mountain passes. Driving the winds is the pressure gradient between the cool Pacific and the interior hot Mojave Desert. These winds are part of the sea breeze diurnal cycle and begin late afternoon. Thus, transport depends on both marine and interior conditions. As such, the persistence of the cool coastal marine layer plays a key role. Whereas climate change will increase interior temperatures, there is significant uncertainty in potential impacts on the coastal marine layer.

Furthermore, regional temporal trends cannot be extrapolated to the future without considering global temporal trends, specifically, increasing O_3 transport from Asia (Jacob et al., 1999; Lin et al., 2017) and warming climate. Both microbial production (Hristov et al., 2011) and partitioning between ammonia nitrate particulate and gas phase

NH_3 (Dawson et al., 2007) show positive relationships between emissions and temperature. Thus, warmer climate scenarios likely will increase emissions. Additionally, wildfire activity and resultant emissions are predicted to increase (Westerling and Bryant, 2008). Meanwhile, Mojave Desert warming exacerbates stresses on the desert ecosystem (Lovich and Bainbridge, 1999). For example, upslope migration of vegetation already is observed (Kelly and Goulden, 2008). Equally important will be changing rain and cloud patterns that also stress the desert ecosystem. Significant precipitation decreases shift desert flora towards more drought-tolerant species, while increased precipitation increases the invasion of non-desert species, particularly grasses (Lovich and Bainbridge, 1999), which increase the frequency of fires (Allen et al., 2014). Timing of precipitation and cloudiness are important, affecting evaporation and soil dryness - both likely will change under warmer climate scenarios. To summarize, the desert ecosystem is particularly susceptible to the impacts of climate change, with the Mojave Desert also facing stress from LAB and SJV and wildfire pollution inputs.

4.4. Future work

Despite a thorough literature search, surprisingly few air quality studies were found for the Mojave Desert. This likely is due to its remoteness, low population, and that significant air quality issues remain in other, heavily and densely populated California air basins. Nevertheless, the Mojave Desert is a highly sensitive ecosystem with many endangered species (Jiménez and Dudhia, 2011) facing significant stresses from air pollution, climate change, and expanding human activities. From a regulatory point of view, improvements in Mojave Desert air quality require improvements in air quality in the LAB and SJV air basins. Given that Mojave Desert air quality is a mixture of these sources (and wildfires), which depends on transport, regulations for the LAB and SJV should account for the more complicated chemistry in the downwind Mojave to protect its ecosystem.

As Trijonis et al. (1988) noted, there are strong seasonal variations in air quality in the Mojave Desert due to seasonality in sources, chemistry, and transport. Thus, an atmospheric chemistry field campaign to measure air quality of trace gas and aerosol pollutants and their transport is needed spanning multiple seasons. Airborne measurements along the lines of the NASA AQ field campaign studies (e.g., Discover AQ - Anderson et al. (2014)) are needed. These measurements should be supplemented with more frequent (due to lower logistical costs), mobile surface surveys and fixed station data. Still, field campaigns only provide localized snapshot characterization of Mojave Desert air quality given the significant heterogeneity and gradients in air pollution (Parrish et al., 2017). Thus, both modeling and satellite data analysis should be included in future studies – as herein. Numerical modeling and satellite data also can address the export of Mojave Desert air pollution to the Sonoran Desert and other downwind regions. Finally, ecosystem observations and analysis should be incorporated to characterize air quality by its impacts on the fragile and endangered desert ecosystem.

5. Conclusion

Los Angeles Basin (LAB) and San Joaquin Valley (SJV) air pollution are known significant contributors to poor Mojave Desert air quality. In this study, field campaign data were collected on 19 August 2015 that found important inputs also can arise from distant wildfires in northern California. This was confirmed by numerical modeling and analysis of satellite aerosol data and airborne aerosol lidar data. Given that wildfires are forecast to increase in occurrence and intensity and persistence under warmer climate change scenarios, wildfire air pollution inputs will become increasingly important to the poor air quality of the Mojave Desert (second worst in California).

The current paucity of Mojave Desert air pollution studies argues for further field research. Such research would be of benefit to other desert air basin(s) downwind from megacities globally, which like the Mojave Desert are fragile and highly sensitive ecosystems that is increasingly affected by growing urban areas and industrial activities upwind.

Data availability

Data will be provided as per the data policy.

Author contribution

I. Leifer prepared the manuscript with input from all co-authors. C. Melton prepared figures and conducted data analysis. M. Fischer contributed numerical modeling. L. Iraci, J. Marrero, J-M. Ryoo, T. Tanaka, and E. Yates are part of the AJAX team and worked to collect and analyze AJAX data, W. Gore and M. Fladeland contributed to data collection, B. Chatfield analyzed satellite aerosol data. J. Yorks and D. Hvalaka contributed airborne aerosol profile data.

Data collection and analysis and figure preparation was by Ira Leifer, Christopher Melton, Denis L. Hlavka, Laura Iraci, Josette Marrero, Ju-Mee Ryoo, Tomoaki Tanaka, Emma Yates, John Yorks.

Numerical modeling was by Xinguang Cui and Marc L. Fischer.

Remote Sensing analysis was by Robert Chatfield, Denis L. Hlavka, and John Yorks.

Writing and editing was by all authors, Ira Leifer, Christopher Melton, Robert Chatfield, Xinguang Cui, Marc L. Fischer, Matthew Fladeland, Warren Gore, Denis L. Hlavka, Laura Iraci, Josette Marrero, Ju-Mee Ryoo, Tomoaki Tanaka, Emma Yates, John Yorks.

Declaration of competing interest

The authors declare that they have no known competing financial interests or personal relationships that could have appeared to influence the work reported in this paper.

Acknowledgement

We thank the NASA Earth Science Division, Research and Analysis Program, grant NNX13AM21G. MLF was supported by a grant from the California Energy Commission's Natural Gas Research Program to the Lawrence Berkeley National Laboratory under contract DE-AC02-36605CH11231. AJAX data were collected under the AJAX project, which acknowledges the partnership of H211, LLC and support from the Ames Research Center Director's funds. Josette E. Marrero's funding was provided by the NASA Postdoctoral Program.

Appendix A. Supplementary data

Supplementary data to this article can be found online at https://doi.org/10.1016/j.atmosenv.2019.117184.

References

Ahmadov, R., McKeen, S., Trainer, M., Banta, R., Brewer, A., Brown, S., Edwards, P.M., de Gouw, J.A., Frost, G.J., Gilman, J., Helmig, D., Johnson, B., Karion, A., Koss, A., Langford, A., Lerner, B., Olson, J., Oltmans, S., Peischl, J., Pétron, G., Pichugina, Y., Roberts, J.M., Ryerson, T., Schnell, R., Senff, C., Sweeney, C., Thompson, C., Veres, P.R., Warneke, C., Wild, R., Williams, E.J., Yuan, B., Zamora, R., 2015. Understanding high wintertime ozone pollution events in an oil-and natural gas-producing region of the western US. Atmos. Chem. Phys. 15, 411–429.

Alexander, C.R., Weygandt, S.S., Benjamin, S.G., Mirnova, T.G., Brown, J.M., Hofmann, P., James, E., 2011. Recent and Future Enhancements, Time-Lagged Ensembling, and 2010 Forecast Evaluation Activities, 24th Conference on Weather and Forecasting/20th Conference on Numerical Weather Prediction. American Meteorological Society, Seattle, WA, p. 12, 12B.

Allen, M.F., Barrows, C.W., Bell, M.D., Jenerette, G.D., Johnson, R.F., Allen, E.B., 2014. Threats to California's desert ecosystems. Fremontia, J. Calif. Nativ. Plant Soc. 42, 3–7.

American Lung Association, 2019. State of the Air. American Lung Association, Chicago, IL, p. 167, 2016.

Anderson, D.C., Loughner, C.P., Diskin, G., Weinheimer, A., Canty, T.P., Salawitch, R.J., Worden, H.M., Fried, A., Mikoviny, T., Wisthaler, A., Dickerson, R.R., 2014. Measured and modeled CO and NOy in DISCOVER-AQ: an evaluation of emissions and chemistry over the eastern US. Atmos. Environ. 96, 78–87.

Bao, J.W., Michelson, S.A., Persson, P.O.G., Djalalova, I.V., Wilczak, J.M., 2008. Observed and WRF-simulated low-level winds in a high-ozone episode during the Central California Ozone Study. J. Appl. Meteorol. Climatol. 47, 2372–2394.

Bastable, H.G., Rogers, D.P., Schorran, D.E., 1990. Tracers of opportunity and pollutant transport in Southern California. Atmos. Environ. Part B - Urban Atmos. 24, 137–151.

Chen, F., Dudhia, J., 2001. Coupling an advanced land surface–Hydrology model with the Penn State–NCAR MM5 modeling system. Part II: preliminary model validation. Mon. Weather Rev. 129, 587–604.

Chen, H., Winderlich, J., Gerbig, C., Hoefer, A., Rella, C.W., Crosson, E.R., Van Pelt, A.D., Steinbach, J., Kolle, O., Beck, V., Daube, B.C., Gottlieb, E.W., Chow, V.Y., Santoni, G. W., Wofsy, S.C., 2010. High-accuracy continuous airborne measurements of greenhouse gases (CO_2 and CH_4) using the cavity ring-down spectroscopy (CRDS) technique. Atmos. Meas. Tech. 3, 375–386.

Clarisse, L., Shephard, M.W., Dentener, F., Hurtmans, D., Cady-Pereira, K., Karagulian, F., Van Damme, M., Clerbaux, C., Coheur, P.-F., 2010. Satellite monitoring of ammonia: a case study of the San Joaquin Valley. J. Geophys. Res. 115.

Cox, P., Delao, A., Komorniczak, A., 2013. Background Material: Almanac of Emissions and Air Quality, 2013 Edition. California Air Resources Board, Sacramento, CA.

Cui, X., Newman, S., Xu, X., Andrews, A.E., Miller, J., Lehman, S., Jeong, S., Zhang, J., Priest, C., Campos-Pineda, M., Gurney, K.R., Graven, H., Southon, J., Fischer, M.L., 2019. Atmospheric observation-based estimation of fossil fuel CO_2 emissions from regions of central and southern California. Sci. Total Environ. 664, 381–391.

Dawson, J.P., Adams, P.J., Pandis, S.N., 2007. Sensitivity of PM2.5 to climate in the Eastern US: a modeling case study. Atmos. Chem. Phys. 7, 4295–4309.

Gentner, D.R., Ford, T.B., Guha, A., Boulanger, K., Brioude, J., Angevine, W.M., de Gouw, J.A., Warneke, C., Gilman, J.B., Ryerson, T.B., Peischl, J., Meinardi, S., Blake, D.R., Atlas, E., Lonneman, W.A., Kleindienst, T.E., Beaver, M.R., Clair, J.M.S., Wennberg, P.O., VandenBoer, T.C., Markovic, M.Z., Murphy, J.G., Harley, R.A., Goldstein, A.H., 2014. Emissions of organic carbon and methane from petroleum and dairy operations in California's San Joaquin Valley. Atmos. Chem. Phys. 14, 4955–4978.

Hong, S.-Y., Noh, Y., Dudhia, J., 2006. A new vertical diffusion package with an explicit treatment of entrainment processes. Mon. Weather Rev. 134, 2318–2341.

Hristov, A.N., Hanigan, M., Cole, A., Todd, R., McAllister, T.A., Ndegwa, P.M., Rotz, A., 2011. Review: ammonia emissions from dairy farms and beef feedlots. Can. J. Anim. Sci. 91, 1–35.

Jacob, D.J., Logan, J.A., Murti, P.P., 1999. Effect of rising Asian emissions on surface ozone in the United States. Geophys. Res. Lett. 26, 2175–2178.

Jeong, S., Hsu, Y.-K., Andrews, A.E., Bianco, L., Vaca, P., Wilczak, J.M., Fischer, M., 2013. Multi-tower measurement network estimate of California's methane emissions. J. Geophys. Res. Atmos. 118, 2013JD019820.

Jerrett, M., Burnett, R.T., Pope, C.A., Ito, K., Thurston, G., Krewski, D., Shi, Y., Calle, E., Thun, M., 2009. Long-term ozone exposure and mortality. N. Engl. J. Med. 360, 1085–1095.

Jiménez, P.A., Dudhia, J., 2011. Improving the representation of resolved and unresolved topographic effects on surface wind in the WRF model. J. Appl. Meteorol. Climatol. 51, 300–316.

Katzenstein, A.S., Doezema, L.A., Simpson, I.J., Blake, D.R., Rowland, F.S., 2003. Extensive regional atmospheric hydrocarbon pollution in the southwestern United States. Proc. Natl. Acad. Sci. 100, 11975–11979.

Kelly, A.E., Goulden, M.L., 2008. Rapid shifts in plant distribution with recent climate change. Proc. Natl. Acad. Sci. 105, 11823–11826.

Krautwurst, S., Gerilowski, K., Krings, T., Borchard, J., Bovensmann, H., Leifer, I., Fladeland, M.M., Koyler, R., Iraci, L.T., Luna, B., Thompson, D.R., Eastwood, M., Green, R., Jonsson, H.H., Vigil, S.A., Tratt, D.M., 2016. COMEX - Final Report: Scientific and Technical Assistance for the Deployment of a Flexible Airborne Spectrometer System during CMAPExp and COMEX, p. 148.

Leen, J.B., Yu, X.Y., Gupta, M., Baer, D.S., Hubbe, J.M., Kluzek, C.D., Tomlinson, J.M., Hubbell 2nd, M.R., 2013. Fast *in situ* airborne measurement of ammonia using a mid-infrared off-axis ICOS spectrometer. Environ. Sci. Technol. 47, 10446–10453.

Leifer, I., Melton, C., Fischer, M.L., Fladeland, M., Frash, J., Gore, W., Iraci, L.T., Marrero, J.E., Ryoo, J.-M., Tanaka, T., Yates, E.L., 2018a. Atmospheric characterization through fused mobile airborne and surface *in situ* surveys: methane emissions quantification from a producing oil field. Atmos. Meas. Tech. 11, 1689–1705.

Leifer, I., Melton, C., Frash, J., Fischer, M.L., Cui, X., Murray, J.J., Green, D.S., 2016a. Fusion of mobile *in situ* and satellite remote sensing observations of chemical release emissions to improve disaster response. Front. Sci. 4, 1–14.

Leifer, I., Melton, C., Manish, G., Leen, B., 2014. Mobile monitoring of methane leakage. Gases Instrum. 20–24. July/August 2014.

Leifer, I., Melton, C., Tratt, D.M., Buckland, K.N., Chang, C., Frash, J., Hall, J.L., Kuze, A., Leen, B., Lieven, C., Lundquist, T., Van Damme, M., Vigil, S., Whitburn, S., Yurganov, L., 2018b. Validation of mobile in situ measurements of dairy husbandry emissions by fusion of airborne/surface remote sensing with seasonal context from the Chino Dairy Complex. Environ. Pollut. 242, 2111–2134.

Leifer, I., Melton, C., Tratt, D.M., Buckland, K.N., Chang, C., Lieven, C., Franklin, M., Hall, J.L., Leen, B., Lundquist, T., Van Damme, M., Vigil, S., Whitburn, S., 2019. Estimating exposure to hydrogen sulfide from animal husbandry operations using satellite ammonia as a proxy: methodology demonstration. Sci. Total Environ. https://doi.org/10.1016/j.scitotenv.2019.134508. In press.

Leifer, I., Melton, C., Tratt, D.M., Buckland, K.N., Clarisse, L., Coheur, P., Frash, J., Gupta, M.X., Johnson, P.D., Leen, B., van Damme, M., Whitburn, S., Yurganov, L., 2016b. Remote sensing and *in situ* measurements of methane and ammonia emissions from a megacity dairy complex: Chino, CA. Environ. Pollut. 221, 37–51.

Levy, R.C., Mattoo, S., Munchak, L.A., Remer, L.A., Sayer, A.M., Patadia, F., Hsu, N.C., 2013. The Collection 6 MODIS aerosol products over land and ocean. Atmos. Meas. Tech. 6, 2989–3034.

Lin, M., Horowitz, L.W., Payton, R., Fiore, A.M., Tonnesen, G., 2017. US surface ozone trends and extremes from 1980 to 2014: quantifying the roles of rising Asian emissions, domestic controls, wildfires, and climate. Atmos. Chem. Phys. 17, 2943–2970.

Lovich, J.E., Bainbridge, D., 1999. Anthropogenic degradation of the Southern California desert ecosystem and prospects for natural recovery and restoration. Environ. Manag. 24, 309–326.

Mazzuca, G.M., Ren, X., Loughner, C.P., Estes, M., Crawford, J.H., Pickering, K.E., Weinheimer, A.J., Dickerson, R.R., 2016. Ozone production and its sensitivity to NOx and VOCs: results from the DISCOVER-AQ field experiment. Atmos. Chem. Phys. 16, 14463–14474. Houston 2013.

McGill, M., Hlavka, D., Hart, W., Scott, V.S., Spinhirne, J., Schmid, B., 2002. Cloud Physics Lidar: instrument description and initial measurement results. Appl. Opt. 41, 3725–3734.

Mesinger, F., DiMego, G., Kalnay, E., Mitchell, K., Shafran, P.C., Ebisuzaki, W., Jović, D., Woollen, J., Rogers, E., Berbery, E.H., Ek, M.B., Fan, Y., Grumbine, R., Higgins, W., Li, H., Lin, Y., Manikin, G., Parrish, D., Shi, W., 2006. North American Regional Reanalysis. Bull. Am. Meteorol. Soc. 87, 343–360.

Nehrkorn, T., Eluszkiewicz, J., Wofsy, S.C., Lin, J.C., Gerbig, C., Longo, M., Freitas, S., 2010. Coupled Weather Research and Forecasting – Stochastic Time-Inverted Lagrangian Transport (WRF–STILT) model. Meteorol. Atmos. Phys. 107, 51–64.

Niccum, E.M., Lehrman, D.E., Knuth, W.R., 1995. The influence of meteorology on the air quality in the San Luis Obispo county-southwestern San Joaquin Valley region for 3-6 August 1990. J. Appl. Meteorol. 34, 1834–1847.

Pandis, S.N., Harley, R.A., Cass, G.R., Seinfeld, J.H., 1992. Secondary organic aerosol formation and transport. Atmos. Environ. Part A. General Topics 26, 2269–2282.

Parrish, D.D., Young, L.M., Newman, M.H., Aikin, K.C., Ryerson, T.B., 2017. Ozone design values in Southern California's air basins: temporal evolution and U.S. background contribution. J. Geophys. Res.: Atmos. 122, 11166–11182.

Pillai, D., Gerbig, C., Ahmadov, R., Rödenbeck, C., Kretschmer, R., Koch, T., Thompson, R., Neininger, B., Lavrié, J.V., 2011. High-resolution simulations of atmospheric CO_2 over complex terrain – representing the Ochsenkopf mountain tall tower. Atmos. Chem. Phys. 11, 7445–7464.

Pinder, R.W., Gilliland, A.B., Dennis, R.L., 2008. Environmental impact of atmospheric NH_3 emissions under present and future conditions in the eastern United States. Geophys. Res. Lett. 35, L12808.

Reible, D.D., Ouimette, J.R., Shair, F.H., 1982. Atmospheric transport of visibility degrading pollutants into the California Mojave Desert. Atmos. Environ. 16, 599–613.

Ruiz, J.J., Saulo, C., Nogués-Paegle, J., 2010. WRF model sensitivity to choice of parameterization over South America: validation against surface variables. Mon. Weather Rev. 138, 3342–3355.

SJVUAPCD, 2015. 2015 Plan for the 1997 PM2.5 Standard. San Joquin Valley Unified Air Pollution Control District, p. 750.

Skamarock, W.C., Klemp, J.B., Dudhia, J., Gill, D.O., Barker, D.M., Huang, X.Z., Wang, W., Powers, J.G., 2008. A Description of the Advanced Research WRF Version 3. National Center for Atmospheric Research, Mesocale and Microscale Meteorology Division, Boulder, Colorado.

Thompson, D., Leifer, I., Bovensman, H., Eastwood, M., Fladeland, M., Frankenberg, C., Gerilowski, K., Green, R., Krautwurst, S., Krings, T., Luna, B., Thorpe, A.K., 2015. Real-time remote detection and measurement for airborne imaging spectroscopy: a case study with methane. Atmos. Meas. Tech. 8, 1–46.

Trijonis, J., McGown, M., Pitchford, M.L., Blumenthal, D., Roberts, P., White, W., Macias, E.S., Weiss, R.F., Waggoner, A.P., Watson, J.G., 1988. RESOLVE Project Final Report: Visibility Conditions and Causes of Visibility Degradation in the Mojave Desert of California. Naval Weapons Center, China Lake, CA, p. 174.

VanCuren, R., 2015. Transport aloft drives peak ozone in the Mojave Desert. Atmos. Environ. 109, 331–341.

Westerling, A.L., Bryant, B.P., 2008. Climate change and wildfire in California. Clim. Change 87, 231–249.